Covalent triazine framework/carbon nanotube hybrids enabling selective reduction of CO2 to CO at low overpotential

ARTICLE

Covalent Triazine Framework/Carbon Nanotube Hybrids: a Novel Class of Electrocatalysts for the Reduction of CO_2

Received 00th January 20xx,
Accepted 00th January 20xx

DOI: 10.1039/x0xx00000x

Andreas Laemont[a], Sara Abednatanzi[a], Parviz Gohari Derakshandeh[a], Florian Verbruggen[b], Erika Fiset[b,], Qing Qin[c], Kevin Van Daele[d,e], Maria Meledina[f,g], Johannes Schmidt[h], Martin Oschatz[c,i], Pascal Van Der Voort[a], Korneel Rabaey[b], Markus Antonietti[c], Tom Breugelmans[d,e] and Karen Leus[a,*]

Electrochemical reduction of CO_2 provides a way to generate base chemicals from an abundant C1-source under mild conditions, whilst at the same time mitigating CO_2 emissions. In this work, a novel class of tailorable, porous electrocatalysts for this process is proposed. Covalent triazine frameworks (CTFs) are grown in situ onto functionalized multiwalled carbon nanotubes. Hydroxyl groups decorating the surface of the multiwalled carbon nanotubes facilitate intimate contact between the carbon nanotubes and CTF, thus promoting efficient electron transfer. The novel hybrid materials generate CO with a Faradaic efficiency up to 81% at an overpotential of 380 mV. The selectivity of the electrocatalysts could be linked to the amount of nitrogen present within the framework.

Introduction

Global warming, caused by anthropogenic CO_2 emission, is without doubt one of the greatest challenges in this century. Despite the increased awareness and efforts so far, the total worldwide anthropogenic CO_2 emissions keep on rising – in 2018 an all-time-high of 37.1 billion metric tonnes of CO_2 was emitted[1]. Carbon capture and utilisation (CCU), i.e. the collection and subsequent conversion of CO_2 into valuable compounds, is expected to become an important mitigation strategy in the near future. Several methods for the conversion of CO_2 are currently under investigation, including biochemical, thermochemical, photochemical and electrochemical routes[2]. In particular electrochemical reduction has been recognized as an efficient and scalable method capable of generating several base chemicals, including carbon monoxide, formic acid and methane from CO_2[3]. The electrochemical reduction can be conducted in aqueous media, which is a cheap, abundant and environmentally friendly way to facilitate the proton and electron transfer steps – although alternative electrolytes are being researched as well[4]. Furthermore, the reaction can be performed under atmospheric pressure and at room temperature. By changing reaction parameters such as the applied potential, electrolyte, electrocatalyst or pH, one can tune the product selectivity towards a desired endproduct and ensure a minimum of by-product formation. Finally, the electricity necessary to drive the reaction can be produced in a renewable manner by e.g. solar power or wind turbines. A widespread industrial implementation however has so far not been realized. To achieve this, improvement of the catalyst cost, current density, overpotential and stability will be necessary[5–9]. The traditional (noble) metal-based catalysts are often expensive or suffer from a poor selectivity due to the competitive and kinetically favoured H_2 evolution side reaction, low electrochemical stability or need for high overpotentials[10–12]. To overcome these shortcomings, a new generation of metal-free electrocatalysts has recently been described, the majority of which is based on nitrogen-doped carbons. Promising findings have been reported proving metal-free catalysts can indeed compete with and in some cases even outperform their metal-based rivals[13–20]. An ideal electrocatalyst should exhibit a high and stable current density at a low overpotential, combined with excellent selectivity towards one specific endproduct.

We introduce the use of covalent organic frameworks (COFs) as suitable candidates for the metal-free electrocatalytic reduction of CO_2. COFs are isoreticular porous networks consisting entirely of light elements linked via a reversible covalent reaction[3]. The chemical properties of the framework depend on the applied monomer and linkage motif, and can be further altered by post-synthetic modifications. Due to their intrinsic porosity, exceptional surface area (up to 4200 m^2/g), well-

[a.] COMOC - Center for Ordered Materials, Organometallics and Catalysis, Department of Chemistry, Ghent University, 9000 Ghent, Belgium.
[b.] CMET- Center for Microbial Ecology and Technology, Department of Biotechnology, Ghent University, 9000 Ghent
[c.] Max Planck Institute of Colloids and Interfaces, Colloid Chemistry, Research Campus Golm, Am Mühlenberg 1, 14476 Potsdam, Germany
[d.] ELCAT – Applied Electrochemistry & Catalysis, Faculty of Applied Engineering, University of Antwerp, 2610 Antwerp, Belgium
[e.] Separation and Conversion Technology, Flemish Institute for Technological Research (VITO), Boeretang 200, Mol 2400, Belgium
[f.] RWTH Aachen University, Central Facility for Electron Microscopy, D-52074 Aachen, Germany
[g.] Forschungszentrum Jülich GmbH, Ernst Ruska-Centre (ER-C 2), D-52425 Jülich, Germany
[h.] Institut für Chemie – Funktionsmaterialien, Technische Universität Berlin, Hardenbergstraße 40, 10623 Berlin, Germany
[i.] Institute of Chemistry, University of Potsdam, Karl-Liebknecht-Str. 24-25, D-14476 Potsdam, Germany
[j.] Electronic Supplementary Information (ESI) available: [^{1}H NMR, FTIR, Raman, XRD, XPS, ADF-STEM-EDX, ICP-MS, LSV, CA,]. See DOI: 10.1039/x0xx00000x
* corresponding author, karen.leus@ugent.be

defined structure and high modularity, COFs find application in a wide range of fields, including adsorption, gas separation and heterogeneous catalysis[21]. In the context of electrocatalytic CO_2 reduction, our interest went in particular to a specific subclass of COFs, denoted as covalent triazine frameworks (CTFs). Based on the stable triazine ring as linkage unit, CTFs exhibit excellent thermal and (electro)chemical stability and can be synthesised in a convenient and straightforward manner. This triazine linkage furthermore results in an inherent high amount of nitrogen present within the CTF structure. Through a rational selection of the monomer, the nitrogen content can be even further increased, or another heteroatom can be introduced. This co-doping of nitrogen-doped carbons with elements such as sulphur, fluorine or boron has indeed proven to ameliorate catalytic performance[22,23]. The customary ionothermal synthesis of CTFs was developed in 2008 by Kuhn et al.[24] and relies on the trimerisation of nitrile-containing monomers at elevated temperatures (> 400°C) in the presence of $ZnCl_2$ as a Lewis acid catalyst. This method yields stable, but amorphous materials, with partial carbonization and irreversible C-N bond formation due to the applied harsh synthesis conditions[25]. The significant amount of defects present in this material and the low degree of crystallinity result into a poor electrical conductivity. For this reason, most reports of CTFs in electrocatalysis describe metallated CTFs, in which the framework acts as a support for the catalytically active metal particles or atoms **[Table 1]**.

For example Su et al. reported in 2018 on a pyridine-based CTF decorated with Co or Ni atoms[26]. While the Co- and Ni-decorated CTFs indeed showed appreciable activity for the reduction of CO_2 to CO, the pristine pyridine CTF exhibited negligible CO generation. In a related work reported by Lu et al. in 2019, Ni was anchored onto a porphyrin-based CTF. The metal-containing CTF favoured the reduction of CO_2 to CO with an excellent FE and current density at a reasonably high electrode potential of -0.9V vs. RHE, but the activity of the bare CTF at the same potential was negligible[27]. Zhu et al. were able to significantly increase the performance of the pyridine-CTF by performing the synthesis at 600°C, effectively pyrolyzing the CTF[28]. This improvement however comes at the cost further disordering of the material, to the point where it can hardly be called a CTF anymore. To the best of our knowledge, the only report of a successful metal-free CTF for the electrocatalytic reduction of CO_2 was reported in 2018 by Wang et al[29]. Their tetrafluoroteraphtalonitrile-based CTF made at 400°C generated methane with an impressive FE of 99.4%, be it with very small current density.

Table 1 - An overview of CTFs in electrochemical CO_2 reduction

Material	Potential vs. RHE (V)	Current density (ma/cm²)	F.E.	Ref
Co@pyCTF	-0.8	-1.0	75% CO	26
Ni@pyCTF	-0.8	-1.0	90% CO	26
pyCTF	-0.8	> -0.05	<5% CO	26
Ni@porphyrin-CTF	-0.9	-52.9	97% CO	27
porphyrin-CTF	-0.9	-6.20	10% CO	27
py-CTF-400° C	-0.7	> - 0.10	N/A	28
py-CTF-600° C	-0.7	-0.15	82% CO	28
F-CTF-400	-0.8	-0.20	99.3% CH_4	29

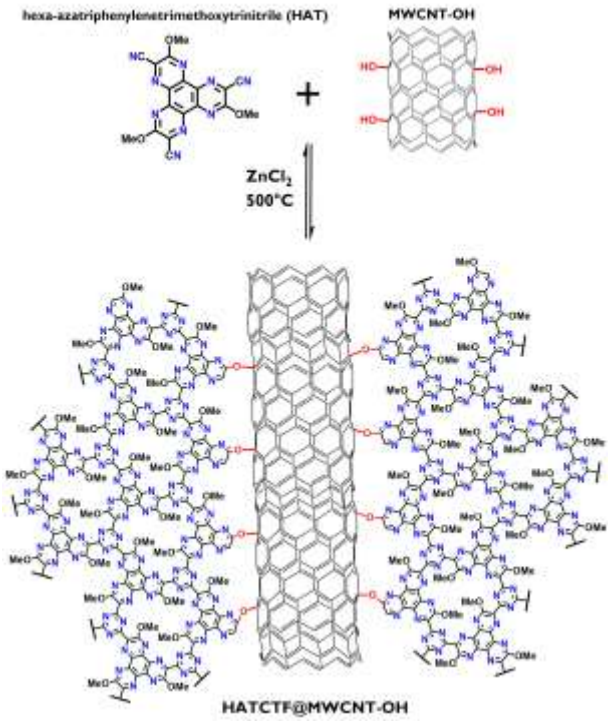

Figure 1: Schematic representation of HATCTF@MWCNT-OH. Note that the exact nature of the bonding between HATCTF and MWCNT-OH is not known.

In this work a novel approach is introduced to overcome the conductivity issue of CTFs by constructing hybrid nanostructures, in which the N-rich CTF will function as the active sites, while the high electrical conductivity will be assured by the functionalized multiwalled carbon nanotubes (MWCNTs) on which the CTFs will be grown onto **[Fig. 1]**. The surface of the multiwalled nanotubes was modified with hydroxyl groups to facilitate the growth of the CTF onto the nanotube and strengthen the contact between both materials, thus improving electron transfer.

Experimental section

Synthesis of MWCNT-OH

The MWCNTs were obtained from Nanocyl SA and used without further purification. For the functionalization of the nanotubes, 1g of the MWCNT was refluxed for 24 hours at 120°C in a 5M nitric acid solution. The product was filtered through a PTFE membrane (0.45 µm), washed with water until the filtrate was pH-neutral, and dried overnight under vacuum. Afterwards, the MWCNT-COOH-OH material was dispersed in 100 mL methanol in a round bottom flask and placed in an ice bath. 5 g of sodium borohydride was added slowly under continuous stirring. After stirring for 24 hours, the product was filtered through a PTFE membrane (0.45 µm), washed with water until the filtrate was pH-neutral and dried overnight under vacuum **[Fig. S1].**

Synthesis of the hexa-azatrimethoxytrinitrile (HAT) monomer

In a first step, hexa-azatriphenylenehexacarbonitrile, HAT-$(CN)_6$ was synthesized according to the published procedure of Czarnik et al[30,31]. For the synthesis of HAT-$(CN)_6$, hexaketocyclohexane octahydrate (4 g, 12.6 mmol) and diaminomaleonitrile (10.88 g, 100.8 mmol) were refluxed in acetic acid (AcOH, 150 mL) for 2 h. The black suspension was filtered off while hot and washed with hot AcOH (3 × 25 mL) resulting in a black solid. The solid was suspended in 30 % HNO_3 (60 mL) and heated at 100 °C for 3 h. The hot dark brown suspension was poured into ice water (200 mL) and cooled overnight. The suspension was filtered and the solid was refluxed in CH_3CN (400 mL) for 2 h and was filtered. The filtrate was evaporated under vacuum to give an orange solid (2.4 g, yield 50 %). In the following step the HAT-$(CN)_6$ (700 mg) was dissolved in CH_3CN (40 mL) followed by the addition of 30 mL CH_3OH, as reported by Chang et al.[32] The reaction mixture was refluxed for 50 hours at 85°C, and left to stand overnight at room temperature. The formed yellow precipitate was filtered. A further crop of product was obtained by adding a few drops of NaOMe to the collected filtrate, until a new precipitation started. The solution was left to stand for an additional 48 hours to precipitate further. The precipitate was filtered, washed extensively with methanol and water, and dried under vacuum overnight. The structure was confirmed using ^{1}H NMR **[Fig. S2]**.

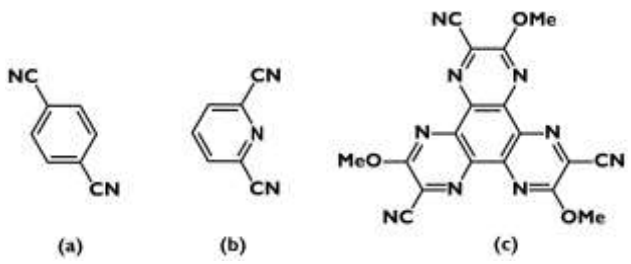

Figure 2: The used monomers: (a) terephthalonitrile, (b) pyridine-2,6-dicarbonitrile and (c) hexa-azatriphenyl-enetrimethoxynitrile for the synthesis of the corresponding hybrid materials CTF1@MWNCT-OH, pyCTF@MWCNT-OH and HATCTF@MWCNT-OH.

Synthesis of the CTF@MWCNT-OH hybrid materials

The monomers (terephthalonitrile (A), pyridine-2,6-dicarbonitrile (B) or hexa-azatrimethoxytrinitrile (HAT) (C), **[Fig. 2]** were thoroughly ground in a mortar in the presence of a twofold mass amount of MWCNT-OH **[Table 1]**. Hereafter, the solid mixture was placed in a glass ampoule, together with an appropriate amount of $ZnCl_2$. Prior to use, the $ZnCl_2$ catalyst was dried at 120°C under vacuum for at least 24 hours. Next, the ampoule was degassed for at least 4 hours, and flame-sealed. For the monomers terephthalonitrile and hexa-azatrimethoxytrinitrile a 5:1 molar ratio of $ZnCl_2$ to monomer was used, while for the pyridine-2,6-dicarbonitrile monomer a 10:1 molar ratio was applied as no surface area was obtained for the latter material when a 5:1 molar ratio was used **[Table 2, Fig. S3]**. The glass ampoules were heated to 500°C (for the pyCTF@MWCNT-OH and HATCTF@MWCNT-OH material) or to 400°C (for the CTF1@MWCNT-OH), and kept at this temperature during 48 hours before cooling down. Afterwards, the glass ampoules were opened, and the obtained black solids were refluxed in 1M HCl at 110°C to remove residual $ZnCl_2$. After 24 hours, the solids were filtered through a PTFE membrane (0.45 µm), and washed with water until the filtrate was pH-neutral. Finally, the hybrid materials were stirred for 24 hours in THF at room temperature, filtered through a PTFE membrane (0.45 µm), washed with THF and acetone, and afterwards dried overnight under vacuum.

Table 2 - An overview of the synthesized hybrid materials under different reaction conditions

Sample	CTF1@ MWCNT-OH	pyCTF@ MWCNT-OH	HATCTF@ MWCNT-OH
Monomer	A*	B*	C*
Amount (mg)	37,5	37,5	33
MWCNT-OH (mg)	75	75	66
$ZnCl_2$ ratio	5:1	10:1	5:1
$ZnCl_2$ (mg)	198	395	56
Temperature (°C)	400	500	500

*A: terephthalonitrile, B: pyridine-2,6-dicarbonitrile, C: hexa-azatrimethoxytrinitrile

Characterization

Nitrogen sorption analysis was conducted at 77 K using an automated gas sorption system Belsorp-Mini II gas analyzer. Prior to the sorption measurements, the samples were dried under vacuum at 120 °C overnight to remove adsorbed water. Specific surface areas were calculated based on Brunauer–Emmett–Teller (BET) analysis. Total pore size was calculated based on Barrett-Joyner-Halenda (BJH) analysis. Elemental analysis was measured on a Thermo Scientific Flash 2000 CHNS-O analyzer equipped with a TCD detector. Powder X-ray diffraction (PXRD) patterns were collected on a Thermo Scientific ARL X'Tra diffractometer, operated at 40 kV, 40 mA using Cu-Kα radiation (1.540 Å). X-ray photoelectron spectroscopy (XPS) measurements were performed on a Thermo Fisher Scientific Escalab 250 Xi. Annular dark field scanning transmission electron microscopy (ADF-STEM) and energy dispersive X-Ray (EDX) spectroscopy experiments were carried out using a FEI Titan transmission electron microscope operated at an accelerating voltage of 200 kV and equipped with a probe spherical aberration corrector unit and a Super-X EDX system[33]. The samples were prepared by dispersing powder samples in ethanol and dropping the dispersion onto a carbon coated TEM copper grid.

Electrochemical tests

The electrochemical performance of the different CTF@MWCNT-OH materials was examined in a gas tight electrochemical cell (H-type configuration), featuring two compartments**,** divided by a proton-permeable Nafion 117 membrane **[Fig. S13].** The cathodic chamber with the glassy carbon working electrode (WE) was filled with 0.1 M $KHCO_3$, saturated with CO_2 (pH = 6.70) in the presence of the Ag/AgCl reference electrode. The anodic chamber was filled with an unsaturated 0.1 M $KHCO_3$ solution in the presence of a platinum counter electrode. The cell was kept at a constant temperature of 18°C by means of water cooling. The WE, counter electrode and reference electrode were coupled to a PARSTAT 4000 potentiostat while the cell headspace was connected to a Thermo-Fisher Scientific TRACE™ 1300 Gas Chromatograph

equipped with a TCD detector. The WE consisted of a glassy carbon rod with a base of 0.2 cm^2, embedded in epoxy in such a way that only the ground plane is available for reaction. The surface was mechanically polished using alumina particles slurry before every reaction to a roughness of 0.05 µm. For each hybrid material, a catalyst ink was prepared, which consisted of 2 mg CTF@MWCNT-OH, 195 µl isopropanol, and 5 µl Nafion® 117 solution (5 wt% in a mixture of lower alcohols). This ink was sonicated for at least one hour to obtain a good dispersion before usage. 20 µl of the ink was dropcasted onto the glassy carbon electrode surface of 0.2 cm^2 in four steps of 5 µl, resulting in a catalyst loading of ca. 1 mg/cm^2. After coating, the electrode was dried overnight in a closed container before usage.

Results and Discussion

To ensure intimate contact between the CTF materials and the MWCNT, hydroxyl functionalities were introduced on the surface of the carbon nanotubes, leading to hydroxyl-functionalized multiwalled carbon nanotubes (MWCNT-OH). This functionalization was achieved by acidic oxidation in a HNO_3 solution according to the reported recipe of Abednatanzi et al[34]. By applying this method, a variety of oxygen-containing species were introduced onto the surface of the nanotube, the majority being carboxyl- and hydroxyl. A subsequent chemical reduction with $NaBH_4$ aimed to convert these carboxyl-groups into hydroxyl groups. A broad O-H stretching band around 3000-3500 cm^{-1}, a C=O stretching vibration around 1720 cm^{-1}, a small O-H bending peak at 1455 cm^{-1}, a C=C stretching around 1570 cm^{-1} and a C-H in-plane bending at 1380 cm^{-1} were observed in the FTIR spectrum of MWCNT-OH, indicating the presence of hydroxyl and carboxyl groups on the surface of the MWCNT **[Fig. S4].** Quantitative XPS analysis indicated circa 3.96 at% of oxygen was present in MWCNT-OH **[Table S1]**.

In the next step, three different hybrid materials were synthesised **[Table 2, Fig. S3]**. For the first material, denoted as CTF1@MWCNT-OH, terephthalonitrile was applied as the monomer which contained no additional nitrogen other than the nitrogen present in the triazine rings. The two other hybrid materials, pyCTF@MWCNT-OH and HATCTF@MWCNT-OH, were built from 2,6-pyridinedicarbonitrile and HAT respectively **[Fig. 1]**. These monomers both contain pyridinic nitrogen. Although this is still under debate, several authors have claimed that the pyridinic nitrogens are the most active sites for CO_2 reduction in nitrogen-doped carbons[18,35]. These hybrid materials were synthesized using the ionothermal method, in which the terminal nitrile groups from three monomers fuse together in a cyclotrimerization reaction to form a triazine ring **[Fig. S3]**. This trimerization reaction relies on the use of high temperatures (400°C or 500°C) depending on the choice of the monomer, in the presence of MWCNT-OH and $ZnCl_2$. For comparison, the bulk HATCTF, pyCTF and CTF1 were also prepared under identical reaction conditions, but in the absence of the MWCNT-OH.

Table 3 – elemental analysis and N_2-sorption results

Name	$A_{s,BET}$ (m^2/g)	V_m (cm^3/g)	N (wt%)	C (wt%)	H (wt%)
MWCNT-OH	263	1.58	0.33	91.92	0.14
CTF1@MWCNT-OH	323	0.34	3.33	87.52	0.70
pyCTF@MWCNT-OH	496	0.41	6.57	77.47	0.66
HATCTF@MWCNT-OH	290	0.76	8.27	81.74	0.67

Elemental analysis indicated a significant increase in the nitrogen content of the hybrid materials in comparison to the pristine MWCNT-OH material which exhibited only 0.33 wt% of nitrogen **[Table 3]**. The highest nitrogen content was observed for the HATCTF@MWCNT-OH material (8.27 wt%), followed by the pyCTF@MWCNT-OH (6.57 wt%) and the CTF1@MWCNT-OH which has a nitrogen content of 3.33 wt%.

DRIFTS measurements of the pristine CTFs showed two broad peaks around 1570 cm^{-1} and 1350 cm^{-1} which we ascribed to the triazine ring vibrations **[Fig. S5]**. As the hybrid materials strongly absorb IR light, little structural information could be derived from their DRIFTS spectra **[Fig. S6]**. A broad D-band at around 1350 cm^{-1} and G-band at around 1600 cm^{-1} could be discerned in the Raman spectra of both the pristine CTFs and the hydrid materials **[Fig. S7, S8].**

In **Fig. 3a** a comparison of the PXRD patterns of the MWCNT-OH, HATCTF and HATCTF@MWCNT-OH is depicted. For all the CTF-based materials a broad (001) diffraction around 2θ = 26° can be observed which can be attributed to a vertical spacing

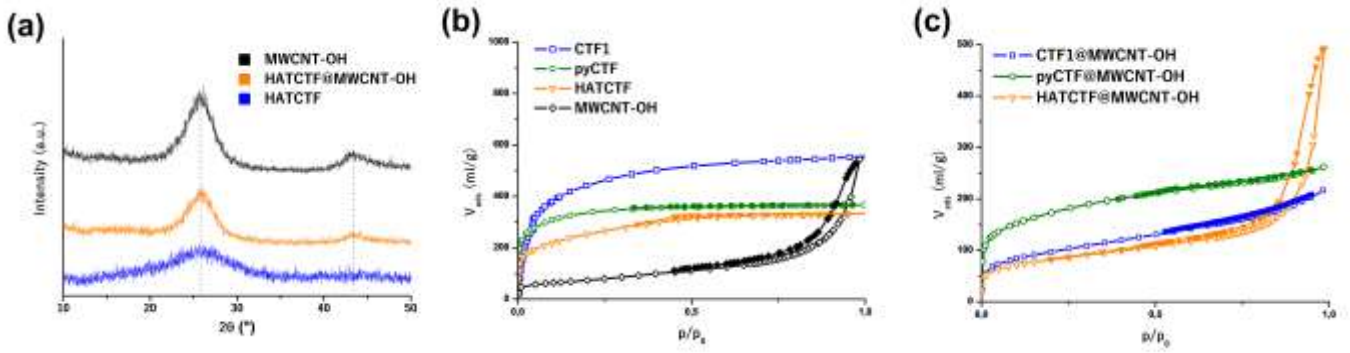

Figure 3: (a) PXRD patterns of MWCNT-OH, HATCTF and HATCTF@MWCNT-OH (b) N_2-physisorption of the MWCNT, CTF1, pyCTF and HATCTF (c) N_2-physisorption of the respective hybrid materials

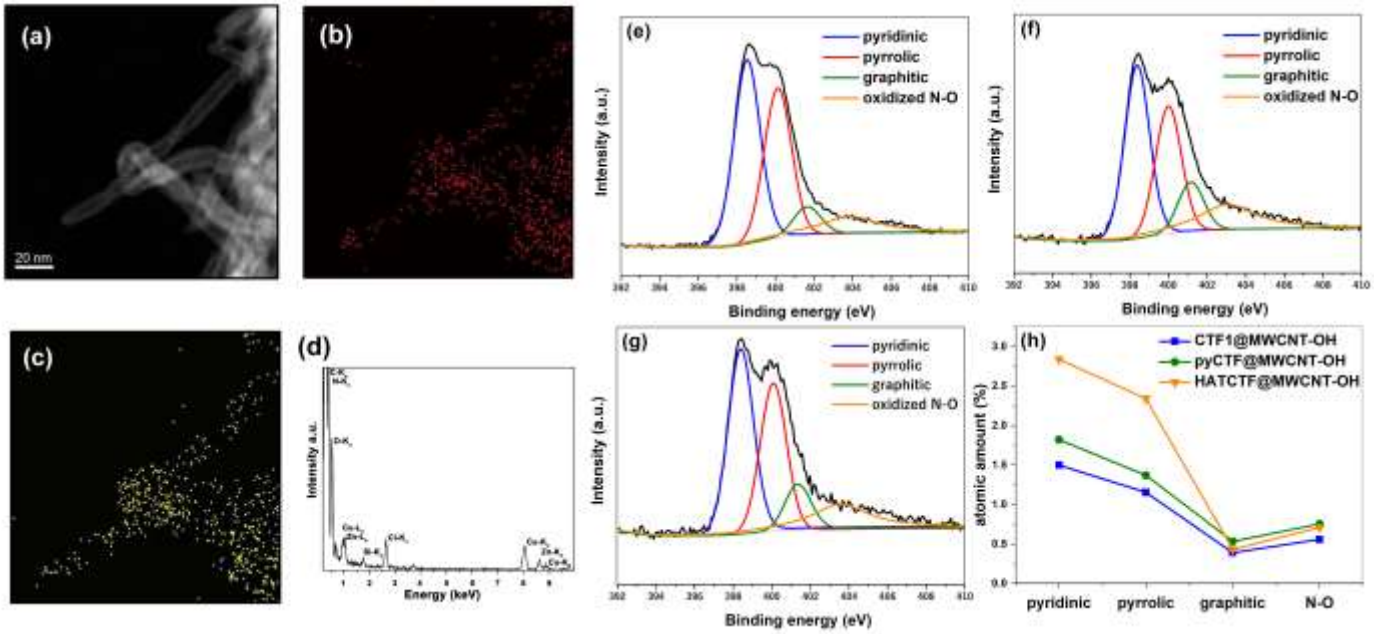

Figure 4: (a) ADF-STEM image of nanotubes in the HATCTF@MWCNT-OH material showing the mapped area together with EDX elemental maps for (b) oxygen, (c) nitrogen and (d) corresponding EDX spectrum with a clear nitrogen signal. (e) Deconvoluted XPS spectrum of the N1S peak of HATCTF@MWCNT-OH, (f) deconvoluted XPS spectrum of the N1S peak of pyCTF@MWCNT-OH, (g) deconvoluted XPS spectrum of the N1S peak of CTF1@MWCNT-OH, (h) atomic nitrogen distribution of HATCTF@MWCNT-OH, pyCTF@MWCNT-OH and CTF1@MWCNT-OH

between the stacked sheets of 3.35 Å[36]. A diffraction at a similar angle is seen in the pristine MWCNT-OH material, which corresponds to the (002) diffraction coming from the interlayer distance between the different concentric single-walled carbon nanotubes that make up a multiwalled carbon nanotube[37]. In addition to this, the MWCNT-OH shows another diffraction at approximately 43°, which can be assigned to the (100) and (101) diffractions in the coiled carbon sheets of carbon nanotubes[37]. This diffraction is not observed in the bulk HATCTF material, but is clearly present in the hybrid HATCTF@MWCNT-OH. The PXRD patterns of CTF1, pyCTF, CTF1@MWCNT-OH and pyCTF@MWCNT-OH can be found in **Fig. S9.**

Further elucidation on the formation of the hybrid materials was found by means of N_2-physisorption measurements **[Fig. 3b,c]**. The bulk CTF materials exhibit a type I isotherm, typical for a microporous material. The functionalized carbon nanotubes on the other hand exhibit a type IV isotherm: in between the randomly entangled carbon nanotubes are voids, where capillary condensation can take place at a p/p_0 values close to one. The isotherm of the HATCTF@MWCNT-OH exhibits both microporosity and capillary condensation, but to a lesser extent than what is observed in the MWCNT-OH material. We postulate that the voids between the carbon nanotubes are filled with CTF. For the pyCTF-MWCNT-OH and CTF1-MWCNT-OH material, capillary condensation is no longer observed at all. A possible explanation lies in the significant difference of the monomers: 128 g/mol and 129 g/mol for terephthalonitrile and 2,6-pyridinedicarbonitrile respectively, versus 399 g/mol for hexa-azatriphenylenetrimethoxytrinitrile. Because for all materials an equal weight ratio of 1:2 monomer to MWCNT-OH was used, the pyCTF@MWCNT-OH and CTF1@MWCNT-OH reaction mixtures contain a larger volume of CTF as compared to HATCTF@MWCNT-OH, enough to entirely fill the voids between the multiwalled carbon nanotubes. The molar amount of hexa-azatriphenylenetrimethoxytrinitrile is not sufficient to entirely fill the mesoporic voids between the carbon nanotubes with HATCTF. This theory is supported by the changes in the BET surface area and total pore volume for the hybrid materials as compared to MWCNT-OH **[Table 3]**. For HATCTF@MWCNT-OH, the decrease in total pore volume is less pronounced than for pyCTF@MWCNT-OH and CTF1@MWCNT-OH. On the other hand, the increase in surface area for the hybrid materials is smaller for HATCTF@MWCNT-OH in comparison to the other hybrid materials. The filling of the mesoporic carbon nanotubes voids by the CTF causes the overall pore volume to decrease, but the BET surface area to increase, with both effects being more pronounced as a higher amount of CTF is present.

A combination of ADF-STEM imaging with EDX elemental mapping was exploited to investigate the morphology and chemical composition of the MWCNT-OH and the hybrid materials. **Fig. S10** contains the ADF-STEM overview and elemental maps for the MWCNT-OH material as well as the EDX spectrum and a HR ADF-STEM image of the multiwalled nanotubes functionalised with –OH groups. A clear oxygen signal is detected for the material and the oxygen distribution nicely correlates to the carbon distribution evidencing the –OH functionalisation of the carbon nanotubes which is in good agreement with the FTIR measurement results. The MWCNT-OH retained the classical multiwalled morphology **[Fig. S10e].** Furthermore, the hybrid materials were subjected to an investigation at the same conditions. **Fig. S11** contains an ADF-STEM overview and the elemental maps for

the HATCTF@MWCNT material. A higher agglomeration of the nanotubes is typical for the HATCTF-functionalised material in comparison to the –OH-functionalised nanotubes. Most probably this effect is related to the ability of the HATCTF to fill in the space between the nanotubes. **Fig. 4a** depicts an ADF-STEM image of the HATCTF-functionalised multiwalled nanotubes, while **Fig. 4b,c** show the correlating presence of respectively oxygen and nitrogen in HATCTF@MWCNT-OH, indicating the growth of nitrogen-rich HATCTF onto the carbon nanotube surface via oxygen linkages. A clear nitrogen signal in the EDX spectrum taken from a few nanotubes shown in Fig. 4a is detected **[Fig. 4d]**. It is evidencing the nitrogen presence in and around the nanotubes of HATCTF@MWCNT rather than a separate nitrogen-containing phase intermixing into agglomerates with nanotubes. No secondary phases were observed also indicating the decoration of the MWCNT-OH by the HATCTF and creation of the hybrid material. In **Fig. S11**, the ADF-STEM image showing the mapped area together with elemental maps, EDX spectrum and HR ADF-STEM image of a single nanotube for the pyCTF@MWCNT-OH material are depicted. The EDX spectrum contains clear peaks of both nitrogen and carbon, while the morphology of a single nanotube still stays regular **[Fig. S11f]**. The distribution of oxygen and nitrogen signals come in agreement revealing the functionalisation of the multiwalled nanotubes **[Fig. S11b,c,d]**.

XPS analysis of the hybrid materials indicated the presence of four distinct types of nitrogen: pyridinic-like nitrogen, pyrrolic-like nitrogen, graphitic nitrogen and oxygenated N-O species **[Fig. 4e,f,g]**. Despite the different monomer, the nitrogen distribution of pyCTF@MWCNT-OH and CTF1@MWCNT-OH show a very similar trend **[Fig. 4h]**. The HATCTF@MWCNT-OH on the other hand is significantly richer in pyridinic and pyrrolic nitrogen, most likely as a result of the monomer, which is rich in pyridinic nitrogen.

Evaluation of the electrocatalytic performance of the CTF@MWCNT based materials

Each hybrid material was coated onto a glassy carbon electrode with a loading of ~ 1 mg/cm^2. The activity in the CO_2 reduction of the hybrid materials was examined by linear sweep voltammetry **[Fig. S14]** and by 200 second chronoamperometry tests at different potentials in a range of -0.5 V to -0.9 V vs. RHE. At every potential an increase in current density was observed for HATCTF@MWCNT-OH in CO_2-saturated 0.1 M $KHCO_3$ as compared to the same electrolyte sparged with argon, indicating the occurrence of electrochemical CO_2 reduction **[Fig. 5a]**. Online GC analysis of the cell headspace during 1800 second chronoamperometry experiments confirmed this statement **[Fig. S16,S17,S18,]**. CO and H_2 could be detected during the reaction in the CO_2-saturated 0.1 M $KHCO_3$ electrolyte at potentials as high as -0.5 V **[Fig. S19,S20,S21,S22,S23]**. The FE for CO in the range of -0.5 V to -0.9 V for all materials is shown in **Fig. 5b** and is maximal at the highest tested WE potential of -0.5V. The rate of the competing hydrogen evolution reaction increases with decreasing WE potential. For all the hybrid materials, the FE for CO generation was maximal at -0.5 V, corresponding to an overpotential of circa 380 mV[11]. A clear correlation between the nitrogen content and the maximal FE at -0.5 V can be noted: while the nitrogen-poor CTF1@MWCNT-OH only produces 41% CO, pyCTF@MWCNT-OH and HATCTF@MWCNT-OH (containing 6.57 wt% and 8.27 wt% nitrogen respectively) generate 60% and 81% CO respectively. Upon shifting to more negative potentials, the CO generation decreased, while at the same time more H_2 was detected by the GC, meaning that lower potentials will foster hydrogen evolution at the cost of CO_2 reduction. The shift from CO to H_2 production happens almost linearly with increasingly negative potential in HATCTF@MWCNT-OH. In CTF1@MWCNT-OH and pyCTF@MWCNT-OH however, the FE for CO decreases less steep. These results can be explained by the observations made by N_2-sorption: HATCTF@MWCNT-OH contains a lower molar ratio of CTF to carbon nanotubes as compared to pyCTF@MWCNT-OH and CTF1@MWCNT-OH. As carbon nanotubes are known to catalyze hydrogen evolution[38], the relatively larger amount of it present in HATCTF@MWCNT-OH will more effectively promote hydrogen evolution at lower potentials. Interestingly, the current densities of HATCTF@MWCNT-OH and CTF@MWCNT-OH are very similar while pyCTF@MWCNT-OH shows more electrochemical activity at every potential **[Fig. 5c]**. This trend does not agree with the nitrogen content as detected by XPS or elemental analysis, but does correlate with the BET surface area: where HATCTF@MWCNT-OH and CTF1@MWCNT-OH show a comparable specific surface area around 300 m^2/g, the increased specific surface area (almost 500 m^2/g) of pyCTF@MWCNT-OH might explain the enhanced activity of this catalyst. **[Table 2]**.

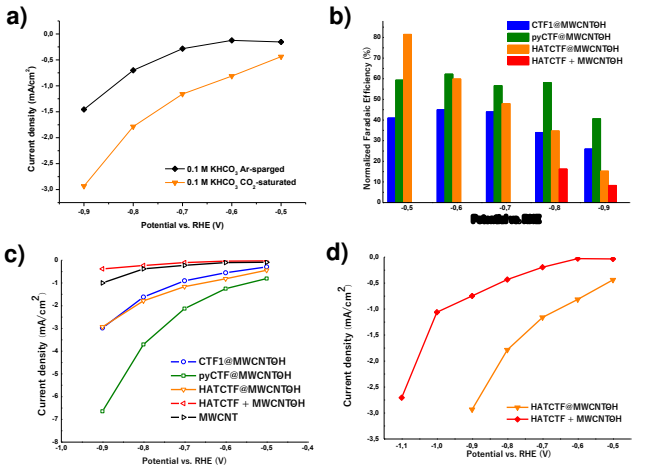

Figure 5: (a) geometric current density of HATCTF@MWCNT- OH in Ar-sparged 0.1 M $KHCO_3$ and CO_2-saturated 0.1 M $KHCO_3$; (b) normalized Faradaic efficiencies for CO of the hybrid materials and HATCTF+MWCNT-OH (c) total geometric current densities of the hybrid materials, HATCTF+MWCNT-OH and MWCNT; (d) geometric current density for HATCTF@MWCNT-OH compared to that of HATCTF+MWCNT-OH

In order to prove the importance of the chemical bonding between the CTF and the carbon nanotube, a blank electrocatalytic test was performed in which a physical mixture of HATCTF and MWCNT-OH was used. More specifically, HATCTF and MWCNT-OH were mixed together in a mortar in a 1:2 weight ratio, denoted as HATCTF+MWCNT-OH. While this sample also contains CTF and MWCNT-OH in the same weight ratio, they are not fused together, as is the case for

HATCTF@MWCNT-OH **[Fig. S24]**. The activity of HATCTF+MWCNT-OH is way smaller than that of HATCTF@MWCNT-OH at every potential **[Fig. 5d].** Hydrogen gas was found to be the main product at -0.8 and -0.9 V **[Fig. 5b]**. Note that at potentials of -0.7 V or higher, the concentration of evolved gasses was below the detection limit of the online GC. Even assuming the unlikely scenario of 100% FE towards CO at -0.5 V for HATCTF+MWCNT-OH, this would still mean the CO current density at -0.5 V of this sample is decreased by more than a factor 10 as compared to the HATCTF@MWCNT-OH.

Impurities of Mn, Fe, Cu and Zn were detected in HATCTF@MWCNT-OH via ICP-MS analysis **[Table S2]**. Mn, Fe and Cu are residual impurities from the synthesis of the carbon nanotubes, while Zn can be ascribed to the $ZnCl_2$ used for the synthesis of HATCTF. Despite extensive efforts we did not succeed in removing these impurities without destroying the catalyst. For these reasons, the catalysts described above cannot strictly be called metal-free. However, two control experiments were undertaken that prove that these impurities are not the source of electrochemical activity for conversion of CO_2 to CO. Consecutive chronoamperometries of pristine multiwalled carbon nanotubes showed that this material exhibits a much lower electrochemical activity, despite also containing metal impurities **[Fig. 5c, S15]**. Online GC detected H_2 as the only gaseous endproduct. As mentioned above, another control experiment was undertaken in which carbon nanotubes were physically mixed but not thermally hybridized with HATCTF, in the same weight ratio as the composition of the catalyst **[Fig. 5d]**. Again, a much smaller current density was detected, however this time also some CO was formed. The combined results of these experiments in our opinion prove that the activity towards CO generation originates from the CTF, and that hybridization with the carbon nanotubes greatly improves the overall activity of the catalyst.

Conclusions

An in situ growth strategy successfully yielded hybrid materials, composed of a layer of CTF grown on functionalized multiwalled carbon nanotubes. The hybrid materials were capable of selective electrochemical conversion of CO_2 to CO. The best results were obtained with HATCTF@MWCNT-OH, achieving 81 % FE at the very low overpotential of 380 mV and with a total current density of -0.48 mA/cm^2. At this overpotential, the HATCTF@MWCNT-OH shows at least a tenfold increase in CO generation activity as compared to a physical mixture of the HATCTF and MWCNT-OH. This observation indicates that the reported novel hybridization method is indeed a viable strategy to use poorly conductive CTFs as part of a functional electrocatalyst, whilst retaining their structural and chemical properties. XPS analysis indicated that the bottom-up synthesis strategy of CTFs offers some degree of control over the nature of the active sites via an adequate choice of monomer. The harsh ionothermal synthesis method however still causes unwanted side-reactions, leading to a range of nitrogen species in the material. The authors of this article will conduct research in the near future towards the use of a mild method for the synthesis of well-defined CTF@MWCNT-OH materials for applications in electrocatalysis.

Conflicts of interest

The authors declare no conflicts of interest.

Acknowledgements

AL acknowledges the financial support from the Ghent University BOF doctoral grant 01D12819. SA acknowledges the financial support from the Ghent University BOF doctoral grant 01D04318. PGD gratefully acknowledges the financial support from the Research Foundation Flanders (FWO-Vlaanderen) grant No. G000117N. KL thanks the financial support from Ghent University. AL thanks dr. Samira Khelifi for the ATR-IRS measurements. The authors acknowledge the funding from the European Union's Horizon 2020 research and innovation programme under grant agreement No. 823717-ESTEEM3.

Notes and references

1 B. Le Quéré, C., Andrew, R. M., Friedlingstein, P., Sitch, S., Hauck, J., Pongratz, J., Pickers, P. A., Korsbakken, J. I., Peters, G. P., Canadell, J. G., Arneth, A., Arora, V. K., Barbero, L., Bastos, A., Bopp, L., Chevallier, F., Chini, L. P., Ciais, P., D, *Glob. Carbon Proj.*, 2018, **4**, 2141–2194.

2 C. Chen, J. F. Khosrowabadi Kotyk and S. W. Sheehan, *Chem*, 2018, **4**, 2571–2586.

3 C. Costentin, M. Robert and J. M. Saveant, *Chem. Soc. Rev.*, 2013, **42**, 2423–2436.

4 P. P. Sharma and X.-D. Zhou, *Wiley Interdiscip. Rev. Energy Environ.*, 2017, **6**, e239.

5 M. Jouny, W. Luc and F. Jiao, *Ind. Eng. Chem. Res.*, 2018, **57**, 2165–2177.

6 J. M. Spurgeon and B. Kumar, *Energy Environ. Sci.*, 2018, **11**, 1536–1551.

7 S. Verma, B. Kim, H. R. M. Jhong, S. Ma and P. J. A. Kenis, *ChemSusChem*, 2016, **9**, 1972–1979.

8 Q.-W. Song, Z.-H. Zhou and L.-N. He, *Green Chem.*, 2017, **19**, 3707–3728.

9 B. Yu, B. Zou and C.-W. Hu, *J. CO2 Util.*, 2018, **26**, 314–322.

10 X. Duan, J. Xu, Z. Wei, J. Ma, S. Guo, S. Wang, H. Liu and S. Dou, *Adv. Mater.*, 2017, **29**, 1–20.

11 W. Zhang, Y. Hu, L. Ma, G. Zhu, Y. Wang, X. Xue, R. Chen, S. Yang and Z. Jin, *Adv. Sci.*, 2018, **5**, 1700275.

12 P. Veerakumar, P. Thanasekaran, T. Subburaj and K.-C. Lin, *C*, 2018, **4**, 54.

13 J. Wu, S. Ma, J. Sun, J. I. Gold, C. Tiwary, B. Kim, L. Zhu, N. Chopra, I. N. Odeh, R. Vajtai, A. Z. Yu, R. Luo, J. Lou, G. Ding, P. J. A. Kenis and P. M. Ajayan, *Nat. Commun.*, 2016, **7**, 1–6.

14 Z. Chen, K. Mou, S. Yao and L. Liu, *J. Mater. Chem. A*, 2018, **6**, 11236–11243.

15 H. Yang, Y. Wu, Q. Lin, L. Fan, X. Chai, Q. Zhang, J. Liu, C. He and Z. Lin, *Angew. Chemie - Int. Ed.*, 2018, **57**, 15476–15480.

16 Y. Liu, S. Chen, X. Quan and H. Yu, *J. Am. Chem. Soc.*, 2015, **137**, 11631–11636.

17 B. Kumar, M. Asadi, D. Pisasale, S. Sinha-Ray, B. A. Rosen, R. Haasch, J. Abiade, A. L. Yarin and A. Salehi-Khojin, *Nat. Commun.*, 2013, **4**, 1–8.

18 H. Wang, J. Jia, P. F. Song, Q. Wang, D. B. Li, S. X. Min, C. X. Qian, L. Wang, Y. F. Li, C. Ma, T. Wu, J. Y. Yuan, M. Antonietti and G. A. Ozin, *Angew. Chemie-International Ed.*, 2017, **56**, 7847–7852.

19 S. Mou, T. Wu, J. Xie, Y. Zhang, L. Ji, H. Huang, T. Wang, Y. Luo, X. Xiong, B. Tang and X. Sun, *Adv. Mater.*, 2019, **31**, 1903499.

20 Y. Zhang, L. Ji, W. Qiu, X. Shi, A. M. Asiri and X. Sun, *Chem. Commun.*, 2018, **54**, 2666–2669.

21 C. S. Diercks and O. M. Yaghi, *Science (80-.).*, 2017, **355**, eaal1585.

22 L. J. Yang, S. J. Jiang, Y. Zhao, L. Zhu, S. Chen, X. Z. Wang, Q. Wu, J. Ma, Y. W. Ma and Z. Hu, *Angew. Chemie-International Ed.*, 2011, **50**, 7132–7135.

23 J. Xie, X. Zhao, M. Wu, Q. Li, Y. Wang and J. Yao, *Angew. Chemie - Int. Ed.*, 2018, **57**, 9640–9644.

24 P. Kuhn, M. Antonietti and A. Thomas, *Angew. Chemie-International Ed.*, 2008, **47**, 3450–3453.

25 D. Y. Osadchii, A. I. Olivos-Suarez, A. V Bavykina and J. Gascon, *Langmuir*, 2017, **33**, 14278–14285.

26 P. Su, K. Iwase, T. Harada, K. Kamiya and S. Nakanishi, *Chem. Sci.*, 2018, **9**, 3941–3947.

27 C. Lu, J. Yang, S. Wei, S. Bi, Y. Xia, M. Chen, Y. Hou, M. Qiu, C. Yuan, Y. Su, F. Zhang, H. Liang and X. Zhuang, *Adv. Funct. Mater.*, 2019, **29**, 1–8.

28 X. Zhu, C. Tian, H. Wu, Y. He, L. He, H. Wang, X. Zhuang, H. Liu, C. Xia and S. Dai, *ACS Appl. Mater. Interfaces*, 2018, **10**, 43588–43594.

29 Y. Wang, J. Chen, G. Wang, Y. Li and Z. Wen, *Angew. Chemie*, 2018, **130**, 13304–13308.

30 K. Kanakarajan and A. W. Czarnik, *J. Org. Chem.*, 1986, **51**, 5241–5243.

31 J. T. Rademacher, K. Kanakarajan and A. W. Czarnik, *Synthesis (Stuttg).*, 1994, **1994**, 378–380.

32 T. H. Chang, B. R. Wu, M. Y. Chiang, S. C. Liao, C. W. Ong, H. F. Hsu and S. Y. Lin, *Org. Lett.*, 2005, **7**, 4075–4078.

33 A. Kovács, R. Schierholz and K. Tillmann, *J. large-scale Res. Facil. JLSRF*, 2016, **2**, 43.

34 M. Masteri-Farahani and S. Abednatanzi, *J. Sci. Islam. Repub. Iran*, 2014, **25**, 27–33.

35 S. Zhang, P. Kang, S. Ubnoske, M. K. Brennaman, N. Song, R. L. House, J. T. Glass and T. J. Meyer, *J. Am. Chem. Soc.*, 2014, **136**, 7845–7848.

36 P. Katekomol, J. Roeser, M. Bojdys, J. Weber and A. Thomas, *Chem. Mater.*, 2013, **25**, 1542–1548.

37 Y. Saito, T. Yoshikawa, S. Bandow, M. Tomita and T. Hayashi, *Phys. Rev. B*, 1993, **48**, 1907.

38 W. Cui, Q. Liu, N. Cheng, A. M. Asiri and X. Sun, *Chem. Commun.*, 2014, **50**, 9340–9342.

